Large-area homogeneous quasifree standing epitaxial graphene on SiC(0001): Electronic and structural characterization

S. Forti,[1,*] K. V. Emtsev,[1] C. Coletti,[1] A. A. Zakharov,[2] C. Riedl,[1] and U. Starke[1,†]

[1]*Max-Planck-Institut für Festkörperforschung, Heisenbergstr. 1, D-70569 Stuttgart, Germany*

[2]*MAXLab, Lund University, P.O. Box 118, Lund, S-22100, Sweden*

(Received 12 July 2011; revised manuscript received 31 August 2011; published 30 September 2011)

The growth of epitaxial graphene on SiC has been identified as one of the most promising techniques to produce graphene for electronic applications. In this paper, we present a systematic study of the electronic and structural properties of large-area quasifree standing epitaxial monolayer graphene grown on top of the SiC(0001) surface. For this purpose, we combine the thermal treatment of SiC in Ar atmosphere to achieve a homogeneous coverage of the surface with the hydrogen intercalation process, which leads to the removal of the interaction between the substrate and the carbon layer. The band structure in the vicinity of the $\overline{\mathrm{K}}$ point is measured using high-resolution angle-resolved photoelectron spectroscopy. A detailed analysis of the quasiparticle dynamics reveals a renormalization of the band velocity estimated to about 3% at energies around 200 meV below the Fermi level, which mainly originates from electron-phonon interaction. Further analysis of the momentum distribution curves leads to the formulation of a model for the doping reduction in such a system in the course of sample annealing above 650 °C. The uniformity and homogeneity of the graphene is demonstrated by means of low-energy electron microscopy (LEEM). Microphotoelectron spectroscopy data confirm the high structural quality and homogeneity of the quasifree standing graphene. Using LEEM and scanning tunneling microscopy, we demonstrate that the hydrogen desorption at elevated temperatures of approximately 750 °C sets in on the graphene terraces rather than via the step edges.

DOI: 10.1103/PhysRevB.84.125449 PACS number(s): 73.22.Pr, 73.20.At

I. INTRODUCTION

Graphene is a single atomic layer consisting of sp^2-hybridized carbon atoms arranged in a honeycomb lattice.[1] It possesses a special kind of electronic structure owing to the linear dispersion relation of its π bands, which are formed by the p_z orbitals of the carbon atoms.[2] In graphene, the π and π^* bands cross without a band gap at the $\overline{\mathrm{K}}$ point of the Brillouin zone. The region around the $\overline{\mathrm{K}}$ point where the electronic dispersion remains linear is usually denominated as the Dirac cone. The crossing point is noted as the Dirac point and its energy as the Dirac energy (E_D). In pristine, undoped graphene, the Fermi energy (E_F) coincides with E_D as sketched in Fig. 1(a), implying that graphene is a semimetal with vanishing charge-carrier density. When the Fermi energy shifts above or below E_D, graphene develops either electron or hole conductivity as sketched in Figs. 1(b) and 1(c), respectively. Due to these remarkable electronic properties, graphene displays some peculiar quantum-mechanical effects,[3] and it has been identified as a promising candidate for future nanoelectronics applications.[4] Nonetheless, the most common technique used in fundamental research for graphene production, namely, mechanical exfoliation from graphite single crystals,[5–7] can provide flakes just a few tens of μm in size. Several other techniques to synthesize graphene have been demonstrated, such as the growth of graphene on metal substrates[8–10] or graphene obtained by chemical exfoliation of graphite.[11] However, the former case necessarily requires the transfer onto an insulating substrate, while graphene obtained by the latter method yields only small crystallites. Rather recently, attempts have been reported to grow graphene by chemical vapor deposition (CVD) on an insulating substrate.[12]

In contrast to other methods, epitaxial graphene grown on silicon carbide[13] (SiC) can be produced directly on a semi-insulating substrate and, hence, does not require any transfer. Moreover, large single-crystal SiC wafers can be readily processed to obtain graphene using existing industrial processing technology. Synthesis of graphene on SiC is achieved by a solid-state decomposition reaction taking place on the surface of SiC upon annealing at elevated temperatures. Under such conditions, Si atoms sublimate from the surface, leaving excessive carbon behind. Decomposition of approximately three SiC bilayers is necessary to crystallize a single layer of graphene on SiC. On the SiC(0001) surface, the first graphenelike carbon layer forms a large unit-cell superstructure with a $(6\sqrt{3} \times 6\sqrt{3})R30^\circ$ periodicity.[14,15] Although having the same geometrical atomic arrangement as graphene, this layer strongly interacts with the substrate via p_z orbitals, so that the π bands typical of graphene can not develop yet.[16] The layer is, therefore, electronically inactive and usually called buffer layer or zero-layer graphene (ZLG). Further annealing at higher temperatures leads to additional accumulation of carbon on the surface, which nucleates into a true monolayer of graphene (MLG) on top of the ZLG. The MLG is electrically active and possesses a typical graphene band structure.[16] Due to charge transfer from the interface, the MLG shows a strong n doping of the order of 10^{13} cm^{-2} as sketched in Fig. 1(b). In the case of strongly doped MLG, renormalization of the energy dispersion due to many-particle interactions was observed in the vicinity of both the Dirac point and the Fermi level (see also Sec. III).[17]

Our group has recently demonstrated that the ZLG can be decoupled from the SiC substrate by hydrogen intercalation.[18] The effect of this method is to remove the covalent interaction between ZLG and substrate. Consequently, the ZLG is turned into quasifree standing monolayer graphene (QFMLG). It was also shown that the process works for few-layer graphene as

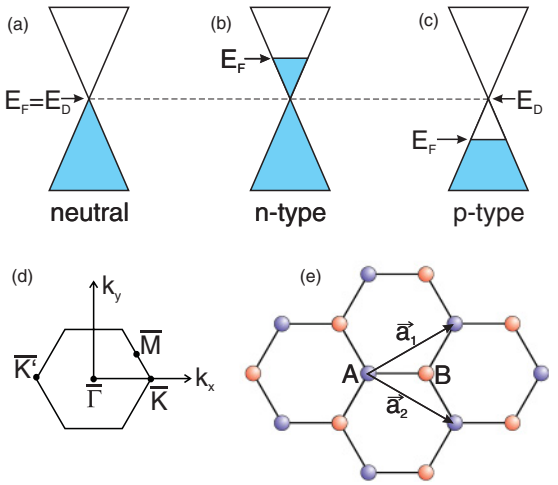

FIG. 1. (Color online) Schematic representation of the π-band dispersion relation for monolayer graphene at (a) charge neutrality, (b) electron doping, and (c) hole doping in the region around the $\overline{K}$ point of the graphene Brillouin zone. The high-symmetry points of the Brillouin zone and the electron momentum coordinates are indicated in (d). Panel (e) represents the real-space graphene lattice. The two inequivalent sites belonging to the two interpenetrating triangular lattices are labeled with A and B, respectively. The unit-cell vectors are indicated with $\vec{a}_1$ and $\vec{a}_2$, where $|\vec{a}_1| = |\vec{a}_2| = a = 2.46$ Å. The distance between two adjacent carbon atoms is $a/\sqrt{3} = 1.42$ Å.

well. In that case, a MLG can be transformed into a quasifree standing bilayer and so on.[18]

In this work, we apply the hydrogen intercalation method to homogeneous zero-layer graphene samples that were obtained by annealing SiC in argon atmosphere.[19] In this way, large-area QFMLG on SiC was produced. We analyze the electronic and structural properties of such high-quality graphene samples in detail. Using angle-resolved photoemission spectroscopy (ARPES), we investigate the quasiparticle dynamics for carrier concentrations close to charge neutrality. Low-energy electron microscopy (LEEM) and micro x-ray photoelectron spectroscopy (μXPS) are used to demonstrate the homogeneity and the quality of the prepared QFMLG. The atomic structure of graphene in QFMLG and ZLG environments is studied by means of scanning tunneling microscopy (STM). The desorption mechanism of hydrogen at elevated temperatures of approximately 750 °C via the graphene terraces is revealed using LEEM and STM.

II. EXPERIMENT

Nominally, on-axis oriented single-crystalline 6H- or 4H-SiC(0001) samples were used in this study, which had been purchased from SiC crystal with *n*-type doping with nitrogen in the range from 10^{17} to 10^{18} cm^{-3}. After dicing and wet chemical cleaning, generally, samples were etched in a flow of hydrogen at a temperature of 1400 °C and pressure of 1 bar in a CVD reactor equipped with a graphite susceptor. The temperature was measured using an infrared pyrometer pointing on the graphite susceptor. With this technique, polishing damage is effectively removed and the resulting surface contains atomically flat terraces of several hundreds

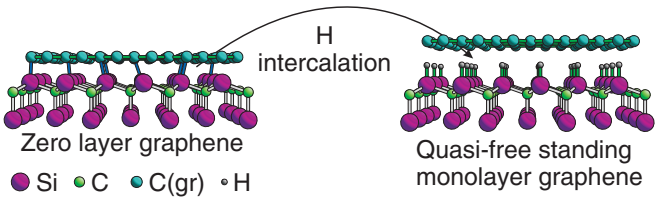

FIG. 2. (Color online) Schematics of the hydrogen intercalation process: As-grown ZLG is covalently bonded to the Si atoms of the topmost SiC layer (left). These bonds are broken when hydrogen intercalates between ZLG and SiC. Hydrogen atoms passivate the Si dangling bonds, so that the carbon layer is decoupled from the substrate. A quasifree standing graphene monolayer forms (right).

of nanometers in width and unit-cell high steps[20] as confirmed by atomic force microscopy (AFM). The particular sample used for the LEEM experiment discussed in Sec. IV was initially flattened by a chemical-mechanical polishing (CMP) process by NOVASIC and, therefore, did not undergo hydrogen etching. It was verified that the pre-treatment method has no significant influence on the morphology and homogeneity of the graphene layers prepared later.

The same reactor was used to graphitize the SiC surfaces by annealing the samples in argon atmosphere. The initial carbon layer (ZLG) forms after annealing at 1400 °C for 10 min and the second carbon layer (MLG) develops at a temperature of 1450 °C after 10 min. This growth technique permits us to grow graphene layers with high uniformity.[19] Successively, the samples were annealed in molecular hydrogen at a pressure close to 1 bar and temperatures around 800 °C. This treatment leads to a hydrogen intercalation resulting in an electronic decoupling of the buffer layer from the substrate.[18] The process is sketched in Fig. 2. The interaction between the ZLG and the substrate is depicted by the Si–C bonds (left side). After the intercalation, these bonds are broken and all Si dangling bonds are passivated with hydrogen (gray balls in the right image). As a result, the ZLG (electrically inactive initially) is turned into a quasifree standing monolayer of graphene.[18]

The electronic band structure of the graphene layers was characterized by ARPES with synchrotron light. The data were acquired using a VG-SCIENTA R4000 photoelectron spectrometer at the SIS-HRPES beamline of the Swiss Light Source (SLS) at the Paul Scherrer Institute (PSI) in Villigen, Switzerland. The resolving power of the spectrometer is $E/\Delta E = 10^4$. Measurements were carried out at a pressure of 2×10^{-11} mbar and at a sample temperature of about 60 K. Samples were illuminated with linearly *p*-polarized and circular polarized light with photon energies in the range from 40 to 90 eV. Valence-band energy dispersion relations as well as constant energy surfaces were acquired in the vicinity of the $\overline{K}$ point of the graphene Brillouin zone. The measurement coordinates within reciprocal space k_x and k_y are indicated in Fig. 1(d).

Structural information about morphology and homogeneity as well as chemical composition of the graphene samples was collected in a combined LEEM and photoelectron emission microscopy (PEEM) experiment using the ELMITEC-LEEM III instrument at the I311 beamline of the MAX-Lab synchrotron radiation facility in Lund, Sweden. The microscope

has a spatial resolution better than 10 nm in the LEEM mode and 30 nm in the PEEM mode. In order to measure LEEM reflectivity spectra, automatic series of LEEM micrographs were acquired with 0.1-eV energy steps. The spectra were subsequently retrieved for constant positions on the surface using a LEED data analysis program. Micro-LEED and micro-XPS measurements were acquired in the diffraction plane of the microscope using small apertures down to 400 nm diameter for μ-LEED and 800 nm for μ-XPS. PEEM and μ-XPS data were acquired using synchrotron radiation. STM measurements were carried out using a Besocke-type instrument with a tungsten tip at room temperature. The STM is contained in a UHV chamber with *in situ* transfer to LEED optics, a sample preparation station, and a load lock. The image analysis was carried out using the WSxM software.[21]

III. ARPES DATA ANALYSIS

The π bands in the vicinity of the $\overline{\mathrm{K}}$ point of the graphene Brillouin zone were compared for as-grown MLG and QFMLG after different annealing stages using high-resolution ARPES. Figure 3 shows energy dispersion plots (E versus $\mathbf{k}_\parallel$) together with the respective Fermi surfaces (placed below each spectrum). For as-grown MLG shown in Figs. 3(a) and 3(e), the carrier density is estimated to $n = (1.0 \pm 0.1) \times 10^{13}$ cm^{-2}, as derived from Fig. 3(a) using the relation $\sigma = \mathbf{k}_\mathrm{F}^2/\pi$, where σ is a two-dimensional (2D) charge density and $\mathbf{k}_\mathrm{F} = (\mathbf{k}_\parallel - \mathbf{k}_{\overline{\mathrm{K}}})$ is the Fermi momentum with respect to the Dirac point [$\mathbf{k}_{\overline{\mathrm{K}}} =$ (1.703, 0) Å^{-1} in the coordinates of Fig. 1(d)]. The band velocity measured close to the Fermi level has been estimated for this system to be $v_F^{\mathrm{MLG}} = (0.90 \pm 0.05) \times 10^6$ m/s. Note that the MLG sample used for the measurements shown in Figs. 3(a) and 3(e) contains a partial contribution of bilayer

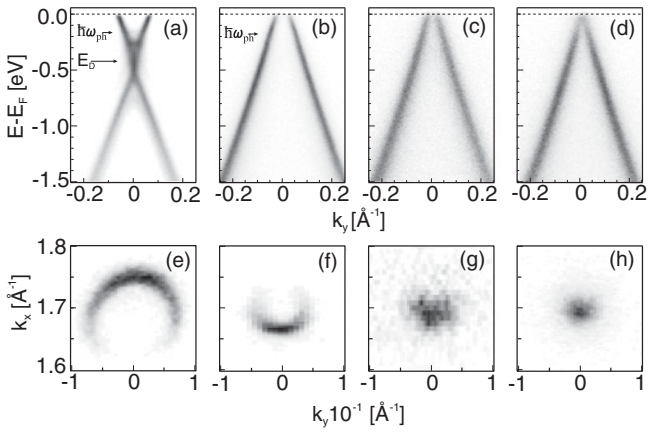

FIG. 3. ARPES spectra of the π bands taken at the $\overline{\mathrm{K}}$ point of the graphene Brillouin zone for (a) as-grown monolayer graphene and (b)–(d) quasifree standing monolayer graphene on the SiC(0001) surface after (b) initial outgassing at 250 °C, (c) annealing at 680 °C and (d) 715 °C, respectively. The spectra were acquired at the $\overline{\mathrm{K}}$ point along the direction perpendicular to the $\overline{\Gamma\mathrm{K}}$ direction in reciprocal space [see Fig. 1(d)]. (e)–(h) Fermi surfaces corresponding to the images shown in (a)–(d), respectively. The photon energy was 90 eV for panels (a)–(g) and 40 eV for panel (h). The light was p polarized for every panel except for panels (c) and (g), where it was circular polarized.

graphene (visible above and below E_D), which originates from the steps[19] as discussed later (Sec. IV).

As reported earlier,[17] deviations from the theoretically predicted linear behavior of the π band near the $\overline{\mathrm{K}}$ point are visible as kinks in the band structure of as-grown MLG, one at energies close to E_D and another around $\hbar\omega_\mathrm{ph} \approx 200$ meV, which corresponds to the energy of the longitudinal optical phonon branch.[22] The former was identified as due to electron-plasmon interactions, the latter to the relaxation of a photohole via emission of a phonon.[17,23] The situation changes if we consider a QFMLG [Figs. 3(b)–3(d) and 3(f)–3(h)]. In this case, the band dispersion is in closer agreement with the linear trend expected for isolated graphene and the measured band velocity amounts to $v_\mathrm{F} = (1.07 \pm 0.05) \times 10^6$ m/s. The achievement of nearly ideal graphene bands has been reported to be possible without any need of decoupling via an intercalation process for graphene grown on the SiC(000$\bar{1}$) surface.[24] Nevertheless, in that case, the system studied was a multilayer epitaxial graphene with a turbostratic arrangement of the layers. Small rotations within individual layers limit the single-crystalline domains to a size of about 1 μm.[24] Our system instead contains truly crystalline single graphene layers on a typical scale of 2–4 μm × 10–20 μm and longer, with a rotation-free periodic arrangement across the entire surface (see Sec. IV).

The only deviation from linearity still observed is visible in Fig. 3(b) as a kink near $\hbar\omega_\mathrm{ph}$. Details of this feature will be discussed below. As seen in Fig. 3(b), the as-prepared and degassed (i.e., after mild annealing in UHV at 250 °C to remove water and organic contaminants from the surface) QFMLG sample displays a slight hole doping (i.e., $E_\mathrm{F} < E_\mathrm{D}$) corresponding to $p = (2.3 \pm 0.1) \times 10^{12}$ cm^{-2}. Interestingly, the hole doping can be reduced by annealing the sample in vacuum at a temperature of 680 °C as seen in Fig. 3(c). Further, after annealing the sample at 715 °C, the Fermi level essentially coincides with the Dirac point, indicating a condition close to charge neutrality. In the latter case, we estimate the charge density to be $p = (3.1 \pm 1.0) \times 10^{11}$ cm^{-2}. This value is rather close to the minimum detectable carrier concentration, which we estimate to be $\approx 1 \times 10^{11}$ cm^{-2}, corresponding to a resolution in momentum space of $\Delta k \approx 0.005$ Å^{-1}.

The appearance of graphenelike π bands in the ZLG after hydrogen intercalation as well as the largely reduced charge-carrier density in the resulting QFMLG as compared to pristine epitaxial MLG provide strong evidence for the decoupling of the layer from the substrate. This can be further corroborated by a closer look at the intensity distribution around the Fermi surfaces. The emission of photoelectrons from the A and B sites in the graphene unit cell [see Fig. 1(e)] can be regarded as a two-source interference phenomenon, bringing as a consequence the fact that the ARPES angular maps exhibit an intensity asymmetry along the constant energy surfaces. In particular, the intensity distribution is such that for p-polarized light, the intensity vanishes on one side of the constant energy surface along the $\overline{\Gamma\mathrm{K}}$ direction.[25] The situation is more complicated if the light is s polarized.[26] On the other hand, the breaking of the A-B symmetry in the graphene lattice should lead to a disruption of the anisotropy of the ARPES angular maps at low energies, resulting in a nonvanishing intensity at all azimuths around the constant energy cuts.[27] An A-B asymmetry, in principle, can be induced by the

interaction between graphene and the substrate and it might lead to the opening of a band gap at the $\overline{\mathrm{K}}$ point.[27,28] Regarding the case of as-grown MLG on SiC(0001), this problem was thoroughly discussed in Ref. 23. Based on the ARPES data analysis, it was concluded that the MLG is not influenced by the substrate and/or the buffer layer[23] and the effect on the MLG is restricted to n doping due to charge transfer from the interface,[29] implying that the MLG does not exhibit a band gap at the $\overline{\mathrm{K}}$ point. The data shown in Figs. 3(a), 3(e), 3(b), and 3(f) indicate the preservation of the A-B symmetry in our graphene. We measured the intensity along the $\overline{\Gamma\mathrm{K}}$ direction for Figs. 3(e) and 3(f), finding $\mathrm{I_{min}/I_{max}} \simeq 6 \times 10^{-3}$ for both. This value is in excellent agreement with what is reported in Ref. 23, and brings us to the conclusion that, despite the lack of any atomic buffer layer between graphene and the substrate in the case of QFMLG, graphene interacts only weakly with the substrate in a sense that its electronic structure is similar to that of a free standing graphene and without observable breaking of the A-B symmetry in the graphene lattice. Apparently, the hydrogen-passivated SiC(0001) surface provides an ideal support for the graphene layer.

As noted above, as-grown MLG shows deviations from a linear band dispersion in the vicinity of the Dirac point [see Fig. 3(a)], which can not be reproduced with a simple single-particle model. In fact, in a recent paper, Bostwick and co-workers showed that, even in a QFMLG epitaxially grown on H-terminated SiC(0001) and subsequently strongly n doped with potassium, a marked renormalization of the energy dispersion exists due to many-particle interactions in the vicinity of the Dirac point.[30] For our case, Fig. 4 shows the ARPES spectrum of an as-prepared QFMLG measured along the $\overline{\Gamma\mathrm{K}}$ direction with a photon energy of 40 eV. The sample, as more clearly visible from Fig. 3(b), displays a slight p doping. At energies around -200 meV with respect to the Fermi level, a small kink in the energy dispersion is observed. Figure 4(a) shows the raw data. In a blown-up region between -0.5 and 0 eV shown in Fig. 4(b), the effect

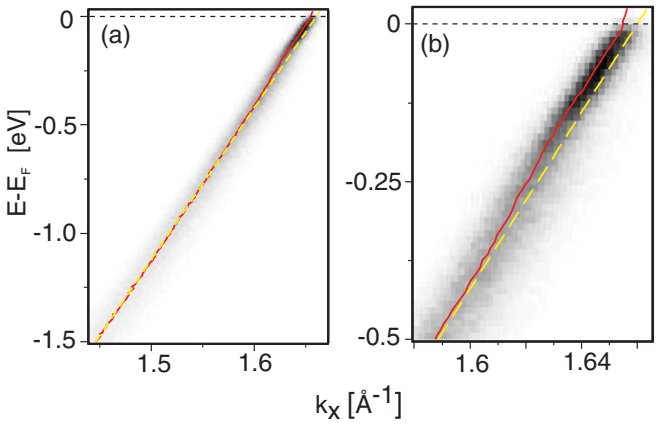

FIG. 4. (Color online) Dispersion of the π bands for a QFMLG sample annealed at 250 °C, taken along the $\overline{\Gamma\mathrm{K}}$ direction at a photon energy of 40 eV. The red solid line represents the position of the maxima of the Lorentzian fits of the MDC's, while the yellow dashed line represents the graphene bare band added to underline the velocity renormalization near ω_{ph}. The raw data [panel (a)] are zoomed in the region between 0 and -0.5 eV in panel (b) to better visualize the kink at around -200 meV.

is even more clearly visible. In both panels, a red (solid) curve superimposed on the spectra reproduces the position of the maxima of the experimental momentum distribution curves (MDC) by means of an algorithm that fits each constant energy line in the ARPES data measured along the $\overline{\Gamma\mathrm{K}}$ direction with a single Lorentzian peak.[31] The yellow (dashed) curve represents instead the graphene bare band [a straight line given by $E = \hbar v_{\mathrm{F}}(k - k_{\mathrm{F}})$], added to better appreciate the velocity renormalization near ω_{ph}.

Within the Fermi-liquid model, the interacting particles are represented as noninteracting quasiparticles with renormalized energy. Following the quasiparticle picture,[17,23] the spectral function measured by ARPES can be expressed in terms of the complex self-energy $\Sigma(\mathbf{k},\omega) = \Sigma'(\mathbf{k},\omega) + i\,\Sigma''(\mathbf{k},\omega)$ as[32]

$$A(\mathbf{k},\omega) = \frac{1}{\pi} \frac{|\Sigma''(\mathbf{k},\omega)|}{\left[\hbar\omega - \varepsilon_{\mathbf{k}}^{0} - \Sigma'(\mathbf{k},\omega)\right]^2 + [\Sigma''(\mathbf{k},\omega)]^2}, \quad (1)$$

where $\hbar\omega$ is the quasiparticle energy and $\varepsilon_{\mathbf{k}}^{0} = \hbar v_{\mathrm{F}}\mathbf{k}$ is the bare band dispersion in the single-particle picture. In the $\mathbf{k}$-independent approximation [i.e., $\Sigma(\mathbf{k},\omega) \approx \Sigma(\omega)$], the width of the ARPES spectrum directly reproduces the imaginary part of the self-energy. We have evaluated experimental ARPES widths as full width at half maximum (FWHM) of the Lorentzian fit curves. The result is plotted as a function of energy in Fig. 5. Figure 5(a) depicts the FWHM of the MDC for an as-grown MLG derived from a spectrum measured along the $\overline{\Gamma\mathrm{K}}$ direction with photons of energy 40 eV. Following Ref. 17, Fig. 5(a) reproduces three main decay processes, namely, the electron-phonon (e-ph) coupling (region I), the electron-hole (e-h) pair generation (regions II and IV), and the emission of plasmons via electron-plasmon (e-pl) coupling (region III). Our data are both qualitatively and quantitatively comparable to what has been reported in literature.[17,23]

Figure 5(b) displays the MDC widths extracted from ARPES data taken along the $\overline{\Gamma\mathrm{K}}$ direction of a QFMLG for different annealing temperatures. The curves have been extracted from spectra measured with photons of energy 40 eV and circular polarization. In fact, we found no correlation between the light polarization and the MDC width. No visible

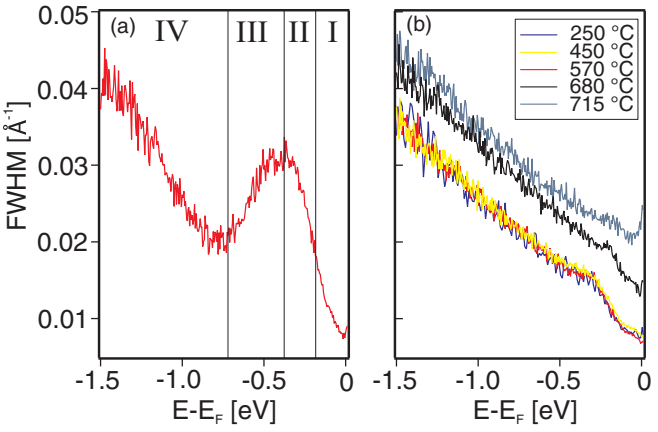

FIG. 5. (Color online) Full width at half maximum (FWHM) of the MDCs measured by ARPES for (a) as-grown MLG with regions of different decay processes indicated (see text for details), and (b) for QFMLG at different annealing temperatures.

difference in MDC widths is observed for samples annealed at temperatures of up to 570 °C as compared to an as-introduced sample. As already pointed out, there is a small kink in the band structure at energies close to $\hbar\omega_{ph}$ [see Figs. 3(b), 3(c) and 4(a), 4(b)]. This is reflected in a humplike structure in the FWHM of the MCDs.

A comparison with Fig. 1(c) of Ref. 33 suggests that the shape of the spectra presented in Fig. 5(b) might be explained by simply considering the electron-phonon interaction. In order to check this, we tried to reproduce the curves in Fig. 5(b) using a corresponding simple model. Since the Einstein model, although more suitable to model the optical phonon branch,[34] gives a null contribution to $\Sigma''(\omega)$ for $\omega < \omega_{ph}$,[35] we considered a zero-temperature isotropic Debye model.[36] In a normal metal, the scattering rate for $\omega > \omega_{ph}$ is energy independent.[35] Hence, we added the contribution given by Eq. (2) of Ref. 33 for $\omega > \omega_{ph}$, accounting in this way for the peculiar band dispersion of graphene.[33] Using the Debye model, the Eliashberg coupling function becomes $\alpha^2F(\omega) = \lambda(\omega/\omega_{ph})^2$ for $\omega < \omega_{ph}$ and zero otherwise.[37] λ is the e-ph coupling parameter and the relation with the imaginary part of the self-energy is $|\Sigma''(\omega)| = \pi\hbar \int \alpha^2F(\omega')d\omega'$. Taking into account these considerations, we express the imaginary part of the self-energy as

$$|\Sigma''(\omega)| = \begin{cases} \hbar\lambda\pi \frac{|\omega|^3}{3\omega_{ph}^2}, & |\omega| < |\omega_{ph}| \\ \hbar\lambda\pi \frac{|\omega_{ph}|}{3} + \frac{\sqrt{3}a^2g^2}{4\hbar v_F^2\epsilon^2}|\omega+\omega_{ph}-\omega_D|, & |\omega| > |\omega_{ph}| \end{cases} \quad (2)$$

where $a = 2.46$ Å is the graphene lattice parameter, g is the unscreened e-ph matrix element measured in eV, $\epsilon = (1 + \epsilon_{SiC})/2 \simeq 3.8$ is the graphene dielectric constant as reported in Ref. 38, $\hbar\omega_D > 0$ is the Dirac energy, $\hbar\omega_{ph} = -198$ meV and, since $E_F = 0$, ω is always negative.[39] To test this model, we applied it to the data shown in Fig. 5(b) as a yellow and black curve (450 °C and 680 °C annealing) and the result is plotted in Figs. 6(a) and 6(b), respectively, by using the relation $\delta k = 2\Sigma''/(\hbar v_F)$.[40] The curve resulting from Eq. (2) is shown in blue in Fig. 6 (label e-ph). The value of λ used to obtain the curve shown in Fig. 6(a) is 0.035, while, for the one in Fig. 6(b), we used 0.03. Nonetheless, since the fitting procedure does not give a univocal and unambiguous result, we estimate the error on λ to be around 30%. For g, we chose 0.53 eV for both curves in order to keep it close to the result given by the *ab initio* calculations,[33] i.e., 0.475 eV. The experimental data are represented by the black dots, and the Dirac energy $\hbar\omega_D$ was set to 180 meV for the curve in Fig. 6(a) and to 140 meV for the one in Fig. 6(b), corresponding to a doping level of $p \simeq 2.3 \times 10^{12}$ cm^{-2} and $p \simeq 1.3 \times 10^{12}$ cm^{-2}, respectively.

Another way to estimate λ is to derive it from the measured band velocity as $\lambda = \frac{v_{ph}}{v_F} - 1$, where v_{ph} is the electron band velocity measured just before the phonon kink.[41] v_{ph} and v_F were determined via a local linear fit of the band dispersion (i.e., the curve reproducing the position of the maxima of the MDCs) taking into account an energy interval of 50 meV (corresponding to 10 points). As a result, we find $\lambda \simeq 0.03$ and the velocity renormalization due to e-ph interaction is therefore estimated to $\sim 3\%$.

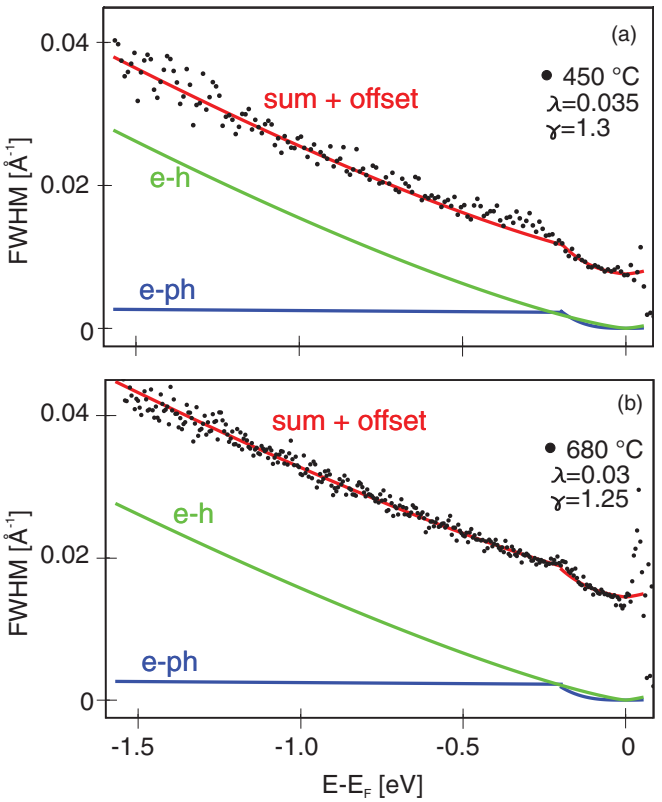

FIG. 6. (Color online) Full width at half maximum (FWHM) of the MDCs measured by ARPES for QFMLG annealed at (a) 450 °C and (b) 680 °C. Solid lines are calculated MDC curves that include (blue) the contribution due to the e-ph interactions using Eq. (2), (green) contribution due to the e-h pair generation decay mechanism, and (red) total sum of the two contributions with an additional offset value of 0.0078 Å^{-1} for (a) and 0.0145 Å^{-1} for (b).

Looking at Figs. 6(a) and 6(b), it appears evident that the model suggested for the e-ph interaction, although modeling in a rather good way the experimental data up to ω_{ph} (aside from a resolution offset as discussed below), it does not provide quantitative agreement, in particular, for energies above the optical phonon emission threshold. To fill this gap, we added a term representing the contribution to the scattering rate arising from the decay of a photohole via e-h pair generation. The result is represented in both panels of Fig. 6 as a green line (labeled as e-h). The process has been modeled using a function of the kind ω^γ, finding $\gamma = 1.3$ as the optimal value for the exponent [Fig. 6(a)], although we tested other exponents up to $\gamma = 1.5$, as suggested in Ref. 17. This supralinear trend appears to be less pronounced at lower doping levels, finding for the data set at 680 °C (black curve in Fig. 5) an optimal fit for $\gamma = 1.25$ albeit, of course, also this parameter is affected by an estimation error.

The red curve in Fig. 6 represents the sum of these two contributions with an additional offset value to take into account the experimental resolution and (possibly) the background due to scattering from impurities and defects. This offset has been set to 0.0078 Å^{-1} in Fig. 6(a) and to 0.0145 Å^{-1} in Fig. 6(b). We note that the data set presented in Fig. 6(b) is rather well reproduced, despite the simplicity of our model here suggested with no need to consider a contribution to the

scattering rate due to the relaxation of a photohole via emission of a plasmon. The data set in Fig. 6(a) reflects a condition of the system where the doping is approximately double to the one in Fig. 6(b), and one observes that the hump is clearly broader. One could explain this broadening with a simple phase-space argument since with the higher doping, the Fermi surface is bigger. Nonetheless, together with the broadening of the peak, a slight energy shift can be observed, possibly implying the presence of a weak plasmon peak at the energy of $\sim$ 300 meV below E_F. We do not have a specific calculation to either confirm or reject this, but we suggest that electron energy loss spectroscopy (EELS) measurements might shine a light on it from an experimental point of view. The fact that a small hump is still observable, even in the charge neutral case, in our opinion, can be explained by considering thermally excited carriers or by simply considering that the system might be not perfectly charge neutral. The further width increment in the spectrum after annealing to 715 °C for energies smaller than $\sim$100 meV is instead an artifact due to the fitting algorithm since, close to the Dirac point, the two branches start to overlap.

By briefly commenting on the reported value of λ, we note that the accuracy of its experimental estimate by means of the relation $\lambda = \frac{v_{ph}}{v_F} - 1$ is always limited by the difficulties in measuring v_{ph}. This is true, in particular, in the case of pristine MLG, where the energy scales of the e-ph and e-pl kinks overlap [see Fig. 3(a)]. The value of v_{ph} measured in this case would therefore be artificially high.[23] For a carrier density of $n = 5.6 \times 10^{13}$ cm^{-2}, the two contributions are instead well separated, and in this case, the value for the e-ph coupling parameter in MLG was reported in Ref. 41 to be about six times larger that the one theoretically predicted through the relation[42]

$$\lambda = 5.55 \times 10^{-9} \sqrt{n}, \tag{3}$$

where n is the carrier density in cm^{-2}. The model that leads to Eq. (3) takes into account the contribution given to λ by the in-plane phonon modes E_{2g} (twofold-degenerate center-zone mode with energy $\simeq$ 195 meV) and A_1' (border-zone mode with energy $\simeq$ 160 meV). We do not have reason to believe that in the QFMLG the phonon modes responsible for λ should be different than in the case of the MLG. The values of λ presented in this paper turn out to be consistent with Eq. (3) multiplied by a factor $\sim$2.5 which, according to Ref. 42, corresponds to the inclusion of resolution effects of the ARPES measurements.

The width of the spectral function is a measure of the quasiparticle lifetime and it is defined as $\tau = 1/(v_F \delta k)$. For an as-introduced QFMLG at $E = \hbar\omega_{ph}$, we find $\tau \simeq 7.6$ fs (the upper limit for a lifetime at $E = E_F$ is $\tau \simeq 11.4$ fs and is of the same order of magnitude as the value calculated in Ref. 42). As visible from Fig. 5(b), there is a direct correlation between the reduction of the doping level and a decrease of the quasiparticle lifetime. A possible explanation might be a partial desorption of H from the interface at higher annealing temperatures. In that scenario, the depassivation of some individual Si dangling bonds at the interface causes an electron transfer from these bonds to graphene as well as an enhanced scattering in graphene. This explanation is further confirmed by noting that there is a definite threshold temperature at about 650 °C below which the band structure remains unaffected. Above that temperature, however, we observe a decrease in the doping level accompanied by a corresponding broadening of the ARPES spectrum.

In Ref. 18, it was suggested that the origin of the doping might possibly be found in the presence of chemisorbed species on the graphene's surface. However, based on our raw data, this appears not likely. Indeed, desorption of adsorbates is clearly evident from the strong enhancement of the intensity and sharpening of the ARPES spectra after annealing the sample at temperatures up to 500 °C. At the same time, no significant doping variation is detected in the band structure itself. On the contrary, as already discussed, the decreasing in the doping level is accompanied by a decrease of the quasiparticle lifetime (broadening of the ARPES spectrum), suggesting that the system has now more scattering centers than before. This can be understood if we consider the situation where an individual Si dangling bond is surrounded by a region of passivated Si atoms. In this scenario, the carbon atom of the graphene layer lying directly above such a dangling bond does not interact with it due to steric hindrance, keeping the graphene in the free standing state. At the same time, such an isolated dangling bond may act as a scattering center and is able to donate charge to the graphene layer. On the other hand, uniform desorption of hydrogen from the surface at $T > 715$ °C locally reestablishes the buffer layer and is manifested by a weakening of the ARPES signal without any further reduction of the graphene doping level.

IV. SURFACE-STRUCTURE ANALYSIS

The spectroscopic analysis in the previous chapter clearly demonstrates that the H-intercalation process transforms the electronically inactive $(6\sqrt{3} \times 6\sqrt{3})R30°$ reconstruction into a quasifree standing graphene monolayer. In the following section, we address the question as to what extent the process yields large-area, homogeneous, and uniformly thick graphene layers, and present further analysis of the structural properties of the QFMLG films. Figure 7(a) displays a LEEM micrograph of a H-intercalated zerolayer sample after outgassing at 550 °C, recorded on a field of view of 25 μm. The image contains large homogeneous terraces of typically 2–4 μm × 10–20 μm size displayed with gray contrast. Even far larger terraces are visible in larger viewfields (not shown). The terraces are separated by thin dark lines. In the inset of Fig. 7(a), a LEEM micrograph taken at 2.2 eV is displayed. Here, the lines appear white in contrast to the dark terraces. Nevertheless, at the particular primary electron energy of 3.0 eV, which was chosen for the main image in Fig. 7(a), certain contrast differences in the form of different gray levels for different terraces can be identified, which requires a more detailed inspection.

Following the work by Hibino *et al.*,[43] the number of pristine graphene layers on SiC(0001) can be determined by means of LEEM reflectivity measurements. It has been shown earlier that this approach can also be used for quasifree standing graphene layers.[18] In Fig. 7(c), LEEM reflectivity spectra (IV curves) are shown acquired from different areas of the sample displayed in Fig. 7(a). Several spectra were measured and display a typical shape for each contrast type, i.e., for the dominating darker and lighter gray areas as well as for the small inclusion of almost white contrast level. Averaged spectra for the area types A, B, and C as indicated

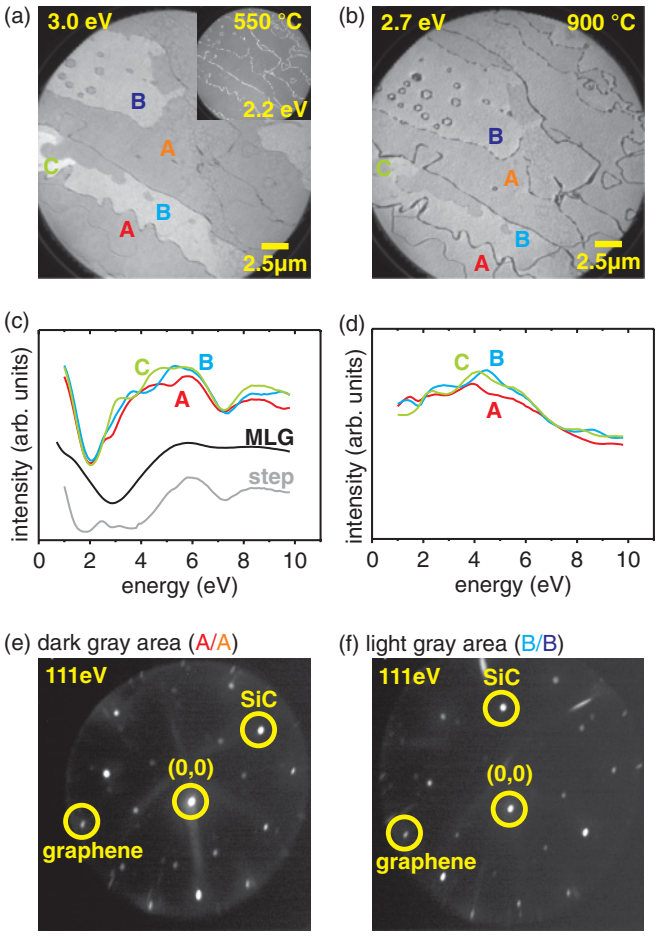

FIG. 7. (Color online) LEEM micrographs of (a) QFMLG outgassed at 550 °C measured with 3.0-eV (inset: 2.2 eV) primary electron energy and (b) after heating to 900 °C where the hydrogen has been desorbed from the sample measured at 2.7 eV. All three images were recorded at the same sample position with a field of view of 25 μm. (c), (d) LEEM reflectivity spectra averaged over areas with similar contrast, i.e., A, B, and C as indicated in panel (a) and (b), respectively. In panel (c), additional spectra are shown as obtained at the dark lines between the QFMLG terraces (indicated step) and for comparison from a pristine graphene monolayer (indicated MLG). (e), (f) Micro-LEED images measured at electron energy of 111 eV of QFMLG outgassed at 550 °C obtained from (e) the dark gray and (f) the light gray areas.

in Fig. 7(a) are displayed in Fig. 7(c) as red, blue, and green curves, respectively. In all cases, a single minimum stands out at an energy of about 2.0 eV, which identifies all gray and white areas as monolayer graphene. Notably, the minimum energy is different from that in pristine MLG on SiC(0001), where the minimum is at about 2.8 eV.[43,44] A corresponding spectrum acquired from a large-area pristine graphene monolayer sample is displayed in black in Fig. 7(c). We note that, for a QFMLG, a further dip appears at 7 eV, which is not developed for pristine MLG, but is also present in quasifree bilayer graphene.[18] Its origin is still not quite understood. However, we note that the interpretation of the dips in the reflectivity spectra as quantum interference peaks of the (multi)layer graphene film relies on the presence of a conduction band between 0 and 7 eV along the ΓA direction in graphite, with band gaps above and below that represent the enclosing Bragg reflection peaks.[43] Therefore, we suggest that the new dip at 7 eV is not connected with the number of layers in the graphene slab, but rather with the detailed structure of the interface. The contrast differences visible in the 3.0-eV LEEM image in Fig. 7(a) are manifested in slight differences in the spectral shape for the different areas. For a closer inspection of their possible origin, we investigated the lighter and darker gray areas by micro-LEED (at a different sample position in order to avoid beam damage). The corresponding diffraction patterns at 111 eV exhibit a threefold symmetry of the SiC-substrate spots as shown in Figs. 7(e) and 7(f). However, the lighter and darker gray regions differ by a rotation of the substrate diffraction spots of 60° with respect to each other. Indeed, on the surface of a hexagonal SiC polytype symmetry, equivalent surface terminations rotated by 60° are possible due to a glide symmetry element present in the bulk unit cell.[45] In addition, the surface can be terminated by different stacking sequences cut out of the bulk sequence. For the $(\sqrt{3}\times\sqrt{3})R30°$ reconstruction on SiC(0001), it has been shown that a surface termination with three bilayers in identical orientation (cubic-type stacking) is favored for both 4H-SiC(0001) and 6H-SiC(0001).[46,47] Therefore, we suggest that also for the $(6\sqrt{3}\times 6\sqrt{3})R30°$ reconstruction (ZLG), a cubic SiC bilayer stacking termination may represent a majority stacking type. The two light and dark gray contrast areas then reflect the 60° rotation of the two possible orientations. For precise normal incidence of the electron beam, no contrast difference should be detected for these domains so that the observed slight deviations have to be attributed to a residual misalignment of the incident electron beam. We note that only a small surface fraction is occupied by patches with white contrast [area C in Fig. 7(a)], which are, however, too small for a micro-LEED analysis. It can be presumed that these areas are characterized by a minority-type SiC stacking termination under the ZLG.

The dark lines visible in the micrographs correspond to the steps of the SiC substrate. As previously reported, the SiC starts to decompose at the step edges,[19] meaning that when a terrace is covered with n layers of graphene, at step edges the formation of the $(n+1)$th layer is observed. Reflectivity spectra taken from the dark lines display two minima at $\approx$1.5 eV and $\approx$4 eV [see Fig. 7(c)], which unambiguously identifies the step areas as quasifree bilayer graphene.[18] Consistent at both electron energies shown in Fig. 7(a), a histogram analysis reveals that the bilayer contribution covers less than 5% of the sample. We note that it is difficult to achieve such a homogeneous coverage for pristine MLG, and indeed data reported in the literature show larger bilayer contributions.[19] Of course, in the case of MLG, two carbon layers have to be grown, which may cause this different behavior.

For the same sample area as displayed in Fig. 7(a), a LEEM micrograph is shown in Fig. 7(b) after annealing to 900 °C when the hydrogen has been desorbed from the surface. Clearly, the morphology of the sample is undisturbed. Even the slight contrast differences can be observed, which were also present in Fig. 7(a). These differences are manifested in slight spectral differences in the LEEM reflectivity curves, as shown in Fig. 7(d) for the same areas A, B, and C

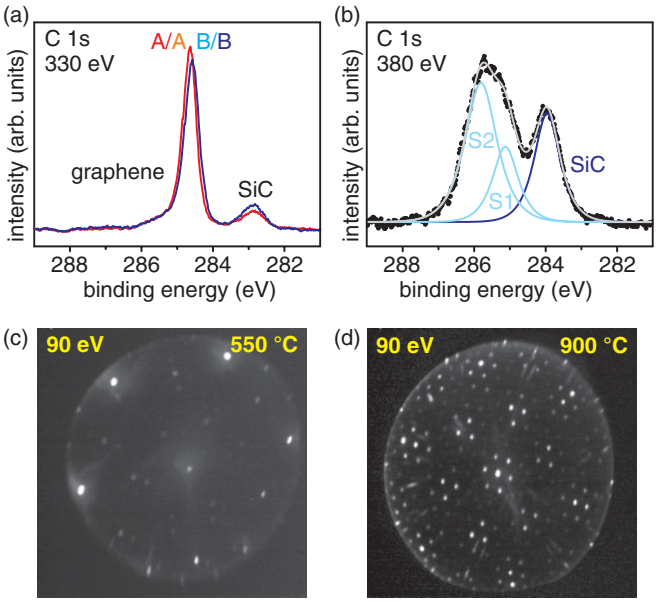

FIG. 8. (Color online) (a), (b) C 1*s* core level spectra measured in the micro-XPS mode from the QFMLG and the hydrogen-desorbed sample stage, respectively. The photon energies are indicated in the respective panels. (c), (d) Micro-LEED images measured at 90 eV from the QFMLG and hydrogen-desorbed sample stages, respectively.

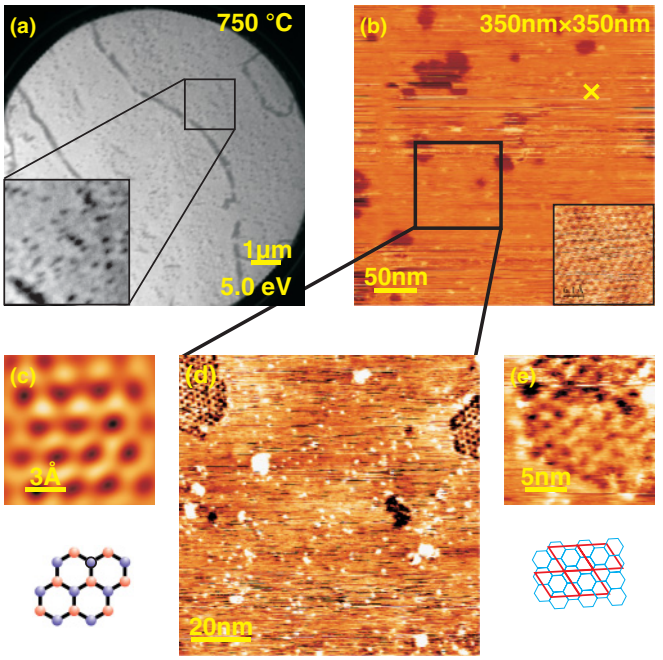

FIG. 9. (Color online) (a) LEEM micrograph of QFMLG after annealing to 750 °C. Electron energy: 5 eV; field of view: 10 μm. Inset: Zoom of the region indicated by the black lines (enhanced contrast, 1.6 × 1.6 μm). (b) STM micrograph of a QFMLG sample showing depressions after partial hydrogen desorption (350 × 350 nm, 2.5 V, 0.3 nA, flattened for spike reduction). Inset: High-resolution scan (3 × 3 nm) showing atomic resolution of graphene (2.0 V, 0.3 nA). (c) Top/left area zoomed from (b) (inset) and FFT filtered (1.1 × 1.1 nm). The graphene atomic structure is sketched below on the same scale. Maximum corrugation: 0.15 Å. (d) Magnified scan within the frame indicated in panel (b), 100 × 100 nm, 2.5 V, 0.3 nA. Depressions of (b) are resolved with the quasi-(6 × 6) periodicity of ZLG. (e) High-resolution scan of the top right depression in panel (d) (18 × 18, 2.5 V, 0.3 nA). The (6 × 6) hexagons and the $(6\sqrt{3} \times 6\sqrt{3})R30°$ unit cell are sketched below on the same scale. Corrugation within depressions ∼1 Å. Average height difference to flat areas ∼0.5 Å.

as indicated in Fig. 7(b) (identical measurement areas as before annealing). However, for all terraces, the minimum typical for monolayer graphene is clearly absent in the IV curves. The spectrum visible is now characteristic for the $(6\sqrt{3} \times 6\sqrt{3})R30°$ reconstruction of carbon atoms on top of the SiC substrate.[43,44]

Further evidence for the extraordinary homogeneity of our graphene film is drawn from a core-level analysis of the different domains by using micro-XPS. The corresponding C 1*s* spectra taken from the gray contrast regions before annealing at a previously unexposed sample position are displayed in Fig. 8(a). Quite evidently, quasifree standing monolayer graphene is present for all measured surface regions since interface components of the $(6\sqrt{3} \times 6\sqrt{3})R30°$ reconstruction can not be detected in the spectra.[18] Note that both contrast types, i.e., A and B in Fig. 7(a), exhibit identical C 1*s* signatures. After hydrogen desorption, the C 1*s* core-level data from micro-XPS give complementary evidence of the back transformation. As shown in Fig. 8(b), the spectrum exhibits the interface components S1 and S2 typical for ZLG with the $(6\sqrt{3} \times 6\sqrt{3})R30°$ reconstruction.[16,48] Finally, a comparison between the micro-LEED patterns of the sample treated with the hydrogen intercalation process and after the hydrogen desorption reveals the decoupling of the QFMLG in contrast to the ZLG. The first-order diffraction spot of graphene and of the SiC substrate are dominating the pattern for QFMLG as shown in Fig. 8(c). Fractional order spots of the $(6\sqrt{3} \times 6\sqrt{3})R30°$ periodicity are fairly weak, which indicates that a reconstruction due to bonds between SiC and graphene is practically absent. The remaining superstructure spots can be explained by double diffraction from the two layers (graphene and SiC). In contrast, in the case of the back-transformed ZLG, the superstructure spots are intense [cf. Fig. 8(d)], which can only be explained by a geometrical restructuring of the graphene layer due to the varying covalent-bond coordination within the $(6\sqrt{3} \times 6\sqrt{3})R30°$ unit cell, which will be also corroborated in the following paragraph.

Following an intermediate annealing step at 750 °C, the modification of the surface can be observed in LEEM using a higher magnification. A corresponding micrograph in Fig. 9(a) displays small black dots developing within the previously homogeneous gray terrace regions (with enhanced contrast in the zoomed inset). A LEEM-IV inspection reveals that the average terrace is still QFMLG, and also the black lines still correspond to quasifree bilayer stripes. Thus, in the main terrace areas as well as in the vicinity of the substrate steps, the majority of the graphene is still decoupled. Only small reacted patches appear on the graphene layer. STM provides insight into the atomic mechanism of the back transformation from QFMLG to ZLG. Figure 9 shows STM micrographs of a sample that had been annealed during the SLS experiments to

a temperature where ARPES and XPS indicate the start of the hydrogen desorption (approximately 750 °C). We emphasize that the samples investigated by LEEM and STM here have been annealed to a higher temperature (750 °C) as compared to the situation where the individual dehydrogenation of Si atoms is indicated by the ARPES analysis in the previous section (715 °C). The sample had been carried through air and only slightly outgassed prior to the STM measurements. Thus, a certain amount of noise is visible caused by residual contaminations. The image in Fig. 9(b) is dominated by flat areas interrupted by depressions of a typical diameter of 20–50 nm or sometimes smaller. As seen in the inset, which displays raw data taken with high resolution in the vicinity of the cross mark, the flat areas can be identified as graphene with a rather low corrugation, much lower than on pristine epitaxial graphene on SiC (MLG).[15] Figure 9(c) displays a magnified area (top/left) of the inset in (b) after fast-Fourier-transform (FFT) filtering.[21] The honeycomb lattice fits perfectly to the atomic structure of graphene as sketched below the STM image. The maximum corrugation as drawn from line profiles is 0.15 Å. In contrast to these flat areas, the darker patches [cf. Fig. 9(b)] display a notably higher corrugation as shown in the high-resolution micrographs in Figs. 9(d) and 9(e). The corrugation in these patches corresponds well to the quasi-(6×6) honeycomb structure of the $(6\sqrt{3} \times 6\sqrt{3})R30^\circ$ periodicity of ZLG. The corresponding arrangement of hexagons within the $(6\sqrt{3} \times 6\sqrt{3})R30^\circ$ unit cell is depicted below the STM image in Fig. 9(e). The corrugation within the quasi-(6×6) grid is of the order of 1 Å. As indicated by the depressionlike appearance of the ZLG patches in Fig. 9(b), the average apparent height of the $(6\sqrt{3} \times 6\sqrt{3})R30^\circ$ grid is approximately 0.5 Å below that of the graphene layer (at the bias voltage of 2.5 V used in the large-scale micrographs). This provides strong indication that the borders between QFMLG and ZLG are caused by the different bonding of the same carbon layer and not by a substrate step, which would contribute a height difference corresponding to the thickness of a SiC bilayer, namely, of 2.52 Å. Note also the shape of the ZLG patches, which is governed by an alignment with the quasi-(6×6) hexagons, which may further hint that the desorption proceeds via the particular registry between the Si atoms of the SiC substrate and the carbon (graphene) layer on top of the (6×6) hexagon lines. We note that, occasionally, dehydrogenation is also observed on small stripes next to SiC substrate steps (not shown). However, the STM measurements indicate that, in the case of QFMLG, the hydrogen desorption takes place mainly on the terraces. Apparently, the hydrogen reaction through a single graphene layer is possible at elevated temperatures in contrast to earlier theoretical predictions.[49,50]

V. CONCLUSION

In conclusion, we demonstrated by means of several surface-analysis techniques that it is possible to efficiently obtain large-area QFMLG on SiC(0001) by combining the thermal treatment of the SiC substrate in Ar atmosphere with the H-intercalation process. Such a graphene closely reproduces the theoretically predicted linear band dispersion for ideal graphene, and the only observable deviation from the linearity at −200 meV with respect to the Fermi level can be mainly assigned to *e*-ph interaction. The scattering rate has been shown to originate from the *e*-*h* pair generation mechanism at high energies, while at low energies, this contribution is comparable to the *e*-ph one. The desorption of hydrogen from individual Si sites of the substrate is suggested as a mechanism to explain the reduction of the doping level with the annealing temperature since it does not imply the covalent interaction between graphene and Si due to steric hindrance. LEEM and STM measurements corroborate this statement. At higher temperatures, hydrogen starts to desorb on the graphene terraces. This is in contrast to theoretical considerations[49,50] and what one observes for thicker graphene films.[18] For a single carbon layer, it may be possible that this proceeds by a stepwise reaction of hydrogen with the carbon lattice via defect configurations, which would be more difficult in a few-layer graphene film. Our work confirms that decoupled epitaxial graphene on SiC is a good candidate for carbon-based electronics.

ACKNOWLEDGMENTS

C.C. acknowledges the Alexander von Humboldt research fellowship for financial support. This research was partially funded by the European Community's Seventh Framework Programme: Research Infrastructures (FP7/2007-2013) under Grant No. 226716. We are indebted to the staff at MAX-Lab (Lund, Sweden) and SLS (Villigen, Switzerland) for their advice and support.

*s.forti@fkf.mpg.de
†u.starke@fkf.mpg.de

[1] H.-P. Boehm, R. Setton, and E. Stumpp, Pure Appl. Chem. **66**, 1893 (1994).
[2] P. R. Wallace, Phys. Rev. **71**, 622 (1947).
[3] A. H. Castro Neto, F. Guinea, N. M. R. Peres, K. S. Novoselov, and A. K. Geim, Rev. Mod. Phys. **81**, 109 (2009).
[4] F. Schwierz, Nat. Nanotechnol. **5**, 487 (2010).
[5] K. S. Novoselov, A. K. Geim, S. V. Morozov, D. Jiang, Y. Zhang, S. V. Dubonos, I. V. Grigorieva, and A. A. Firsov, Science **306**, 666 (2004).
[6] K. S. Novoselov, A. K. Geim, S. V. Morosov, D. Jiang, M. I. Katsnelson, I. V. Grigorieva, S. V. Dubonos, and A. A. Firsov, Nature (London) **438**, 197 (2005).
[7] Y. Zhang, Y.-W. Tan, H. L. Stormer, and P. Kim, Nature (London) **438**, 201 (2005).
[8] X. Li, W. Cai, J. An, S. Kim, J. Nah, D. Yang, R. Piner, A. Velamakanni, I. Jung, E. Tutuc, S. K. Banerjee, L. Colombo, and R. S. Ruoff, Science **324**, 1312 (2009).
[9] S. Bae, H. Kim, Y. Lee, X. Xu, J. S. Park, Y. Zheng, J. Balakrishnan, T. Lei, H. R. Kim, Y. Il Song, Y. J. Kim, K. S. Kim, B. Özyilmaz, J. H. Ahn, B. H. Hong, and S. Iijima, Nat. Nanotechnol. **5**, 574 (2010).

[10]T. Iwasaki, H. J. Park, M. Konuma, D. S. Lee, J. H. Smet, and U. Starke, Nano Lett. **11**, 79 (2011).
[11]C. Gòmez-Navarro, R. T. Weitz, A. M. Bittner, M. Scolari, A. Mews, M. Burghard, and K. Kern, Nano Lett. **7**, 3499 (2007).
[12]W. Strupinski, K. Grodecki, A. Wysmolek, R. Stepniewski, T. Szkopek, P. E. Gaskell, A. Grüneis, D. Haberer, R. Bozek, J. Krupka, and J. M. Baranowski, Nano Lett. **11**, 1786 (2011).
[13]C. Berger, Z. Song, T. Li, X. Li, A. Y. Ogbazghi, R. Feng, Z. Dai, A. N. Marchenkov, E. H. Conrad, P. N. First, and W. A. de Heer, J. Phys. Chem. B **108**, 19912 (2004).
[14]U. Starke, and C. Riedl, J. Phys.: Condens. Matter **21**, 134016 (2009).
[15]C. Riedl, U. Starke, J. Bernhardt, M. Franke, and K. Heinz, Phys. Rev. B **76**, 245406 (2007).
[16]K. V. Emtsev, F. Speck, Th. Seyller, L. Ley, and J. D. Riley, Phys. Rev. B **77**, 155303 (2008).
[17]A. Bostwick, T. Ohta, Th. Seyller, K. Horn, and E. Rotenberg, Nat. Phys. **3**, 36 (2007).
[18]C. Riedl, C. Coletti, T. Iwasaki, A. A. Zakharov, and U. Starke, Phys. Rev. Lett. **103**, 246804 (2009).
[19]K. V. Emtsev, A. Bostwick, K. Horn, J. Jobst, G. L. Kellogg, L. Ley, J. L. McChesney, T. Ohta, S. A. Reshanov, E. Rotenberg, A. K. Schmid, D. Waldmann, H. B. Weber, and Th. Seyller, Nat. Mater. **8**, 203 (2009).
[20]S. Soubatch, S. E. Saddow, S. P. Rao, W. Y. Lee, M. Konuma, and U. Starke, Mater. Sci. Forum **483-485**, 761 (2005).
[21]I. Horcas, R. Fernandez, J. M. Gomez-Rodriguez, J. Colchero, J. Gomez-Herrero, and A. M. Baro, Rev. Sci. Instrum. **78**, 013705 (2007).
[22]L. Vitali, M. A. Schneider, K. Kern, L. Wirtz, and A. Rubio, Phys. Rev. B **69**, 121414(R) (2004).
[23]A. Bostwick, T. Ohta, J. L. McChesney, K. V. Emtsev, Th. Seyller, K. Horn, and E. Rotenberg, New J. Phys. **9**, 385 (2007).
[24]M. Sprinkle, D. Siegel, Y. Hu, J. Hicks, A. Tejeda, A. Taleb Ibrahimi, P. Le Fèvre, F. Bertran, S. Vizzini, H. Enriquez, S. Chiang, P. Soukiassian, C. Berger, W. A. de Heer, A. Lanzara, and E. H. Conrad, Phys. Rev. Lett. **103**, 226803 (2009).
[25]E. L. Shirley, L. J. Terminello, A. Santoni, and F. J. Himpsel, Phys. Rev. B **51**, 13614 (1995).
[26]I. Gierz, J. Henk, H. Höchst, C. R. Ast, and K. Kern, Phys. Rev. B **83**, 121408(R) (2011).
[27]M. Mucha-Kruczyński, O. Tsyplyatyev, A. Grishin, E. McCann, V. I. Fal'ko, A. Bostwick, and E. Rotenberg, Phys. Rev. B **77**, 195403 (2008).
[28]S. Y. Zhou, G.-H. Gweon, A. V. Fedorov, P. N. First, W. A. de Heer, D.-H. Lee, F. Guinea, A. H. Castro Neto, and A. Lanzara, Nat. Mater. **6**, 770 (2007).
[29]S. Kopylov, A. Tzalenchuck, S. Kubatkin, and V. I. Fal'ko, Appl. Phys. Lett. **97**, 112109 (2010).
[30]A. Bostwick, F. Speck, Th. Seyller, K. Horn, M. Polini, R. Asgari, A. H. MacDonald, and E. Rotenberg, Science **328**, 999 (2010).
[31]A. Kaminski and H. M. Fretwell, New J. Phys. **6**, 98 (2004).
[32]S. Hüfner, *Photoelectron Spectroscopy* (Springer, Berlin, 2003).
[33]C. H. Park, F. Giustino, M. L. Cohen, and S. G. Louie, Phys. Rev. Lett. **99**, 086804 (2007).
[34]N. W. Ashcroft and N. D. Mermin, *Solid State Physics* (Brooks/Cole Thomson Learning, USA, 1976).
[35]S. Engelsberg and J. R. Schrieffer, Phys. Rev. **131**, 993 (1963).
[36]S. LaShell, E. Jensen, and T. Balasubramanian, Phys. Rev. B **61**, 2371 (2000).
[37]A. Damascelli, Z. Hussain, and Z. X. Shen, Rev. Mod. Phys. **75**, 473 (2003).
[38]C. H. Park, F. Giustino, C. D. Spataru, M. L. Cohen, and S. G. Louie, Phys. Rev. Lett. **102**, 076803 (2009).
[39]Although it might appear as a pleonastic remark, we note that, for this reason, every inequality in the text between ω and $\omega_{\rm ph}$ have to be regarded as between their respective absolute values, as explicitly expressed in Eq. (2).
[40]In all our discussions, we are neglecting the so-called quasiparticle strength $Z_{n\mathbf{k}}$. We do so because, since it is defined as $Z_{n\mathbf{k}} = 1/(1+\lambda) \simeq 1$, it is not relevant for our discussion.
[41]A. Bostwick, T. Ohta, J. L. McChesney, Th. Seyller, K. Horn, and E. Rotenberg, Solid State Commun. **143**, 63 (2007).
[42]M. Calandra and F. Mauri, Phys. Rev. B **76**, 205411 (2007).
[43]H. Hibino, H. Kageshima, F. Maeda, M. Nagase, Y. Kobayashi, and H. Yamaguchi, Phys. Rev. B **77**, 075413 (2008).
[44]T. Ohta, F. El Gabaly, A. Bostwick, J. L. McChesney, K. V. Emtsev, A. K. Schmid, Th. Seyller, K. Horn, and E. Rotenberg, New J. Phys. **10**, 023034 (2008).
[45]U. Starke, in *Silicon Carbide: Recent Major Advances*, edited by W. J. Choyke, H. Matsunami, and G. Pensl (Springer, Berlin, 2004), pp. 281–316.
[46]U. Starke, J. Schardt, J. Bernhardt, M. Franke, and K. Heinz, Phys. Rev. Lett. **82**, 2107 (1999).
[47]U. Starke, J. Bernhardt, J. Schardt, A. Seubert, and K. Heinz, Mater. Sci. Forum **457-460**, 415 (2004).
[48]C. Riedl, C. Coletti, and U. Starke, J. Phys. D: Appl. Phys. **43**, 374009 (2010).
[49]B. Lee, S. Han, and Y.-S. Kim, Phys. Rev. B **81**, 075432 (2010).
[50]J. Soltys, J. Piechota, M. Lopuszynski, and S. Krukowski, e-print arXiv:1002.4717.